# Snow melt-out date (SMOD) change spanning four decades in European temperate mountains at 30 m from Landsat time series

Arthur Bayle, Simon Gascoin, Christophe Corona, Markus Stoffel, Philippe Choler

scientific data

Check for updates

OPEN

DATA DESCRIPTOR

# Snow melt-out date (SMOD) change spanning four decades in European temperate mountains at 30 m from Landsat time series

Arthur Bayle[1]✉, Simon Gascoin[2], Christophe Corona[1], Markus Stoffel[3,4,5] & Philippe Choler[1]

**Documenting long-term snow cover changes at high spatial resolution is especially challenging in mountain environments due to limited high-elevation ground observations and the coarse resolution of current climate models. This paper presents a dataset of snow melt-out dates (SMOD) at 30-m spatial resolution for two periods—the 1990s (1985–1996) and the 2010s (2011–2022)—across temperate European mountain ranges (Pyrenees, European Alps, and Greater Caucasus), derived from Landsat time series. To address the limited number of observations in the Landsat archive, data were aggregated over 12-year periods, enabling assessment of SMOD changes over four decades at a spatial resolution relevant to above-treeline ecosystems. The SMOD dataset was validated using snow depth station records ($R^2$ ~ 0.75, MAE ~ 7 days) and soil temperature data ($R^2$ ~ 0.7, MAE ~ 10 days) from the Pyrenees and European Alps. Potential applications of the dataset extend beyond alpine ecology, with possible contributions to risk assessments, hydrology, and snow climatology in the context of climate change.**

## Background & Summary

Europe is the fastest-warming continent on Earth with temperatures rising about twice the global average since the 1980s[1]. As snow cover depends on temperature and precipitation, rising temperatures and shifting precipitation patterns are assumed to affect snow abundance[2–4]. Changes in snow cover extent and duration are also expected to alter numerous ecosystem services provided by mountain regions[5]. In above-treeline ecosystems, alpine plant phenology, including the start of growth, peak productivity and senescence is tightly linked to the Snow Melt-Out Date (SMOD)[5,6]. SMOD influences (i) energy availability, as the duration and start of the growing season constrain heat quantity accumulated by plants; (ii) frost exposure, since snow acts as a thermal insulator[7] and (iii) the release of water and nutrient later in the summer[8,9]. Additionally, it conditions interactions within plant communities, particularly in early snow-melting sites where facilitation among species predominates[10]. Because snow accumulation varies spatially along slopes, delayed melting results in a mosaic of environmental conditions over mesotopographic gradients, such ridge-to-snowbed transitions[11,12]. This spatial variability in snow cover and the resulting environmental conditions create great spatial heterogeneity in alpine plant communities, which is a key driver for biodiversity. Thus, snow cover variables (height, melt date, etc.) largely govern interactions between the biosphere and atmosphere, highlighting their crucial role in the response of above-treeline vegetation to climate change.

Studies have identified long-term changes in the snowpack across European temperate mountains[13–18]. Overall, snow cover is receding, but this trend shows strong temporal and spatial variability[19–21]. These patterns are elevation dependent, with the most pronounced changes observed at mid-elevations and more

[1]Univ. Grenoble Alpes, Univ. Savoie Mont Blanc, CNRS, LECA, F-38000, Grenoble, France. [2]Univ. Toulouse, CESBIO, CNES CNRS IRD INRAE UT3 Paul Sabatier, F-31000, Toulouse, France. [3]Climate Change Impacts and Risks in the Anthropocene (C-CIA), Institute for Environmental Sciences, University of Geneva, Geneva, 1205, Switzerland. [4]Department of Earth Sciences, University of Geneva, Geneva, 1205, Switzerland. [5]Department F.-A. Forel for Environmental and Aquatic Sciences, University of Geneva, Geneva, 1205, Switzerland. ✉e-mail: arthur.bayle.env@gmail.com

limited changes at higher elevations[18]. These changes are mainly caused by a rapid upward displacement of the zero-degree isotherm, a shift from solid to liquid winter precipitation[22,23] and by more frequent and intense melting events[24]. Over the last few decades, the trend in snow cover duration and depth has been predominantly negative for periods longer than 30 years, but the trend sign varies over shorter time frames[15]. In the Northern Hemisphere, the most significant changes in snow cover occurred during the 1980s, followed by a hiatus in the 2000s with little or no significant change and in some cases even an increase[25,26]. Similar patterns were found in the European Alps[27–29]. While these studies generally agree on the trajectory of snow cover in European temperate mountains, they rely on either *in situ* observations or climate models, which both are insufficient for characterizing the fine-scale spatial variability of the snowpack and its long-term evolution in response to climate change, specifically at high elevations[18]. Given the highly variable topography of mountain, snow cover duration variability can occur over short distances implying that snow variables need to be tracked at a similar spatial scale to understand the impacts of snow on alpine vegetation[30–32]. However, documenting long-term changes in snow cover duration at high spatial resolution is challenging in mountainous regions, due to the lack of ground observations at high elevations and the limitations of current climate reanalysis in operating at the scale relevant for impact assessments[15,18,33]. According to the IPCC's Special Report on the Ocean and Cryosphere in a Changing Climate (SROCC), trends in solid precipitation at high elevations remain highly uncertain due to inherent limitations in *in situ* observation methods. Identifying these trends is highlighted as a significant research gap[34].

Rather than replacing the above-mentioned approaches, satellite remote sensing offers a complementary approach, providing extensive, high-resolution, and long-duration data on global surface reflectance patterns and trends, from which snow cover variables can be derived[28,35,36]. Specifically, satellite remote sensing is efficient in deriving snow cover absence and presence at a given time and space, providing the basis to estimating snow cover duration. However, the spatial and temporal scales at which snow cover can be described vary depending on the satellite constellation used. For instance, the Sentinel-2 constellation offers high spatial resolution images globally with a short measurement interval, but its temporal coverage of $< 10$ years limits our ability to draw long-term conclusions about snow cover changes. Conversely, the AVHRR constellation provides 40 years of daily reflectance measurements globally, but the kilometer-scale spatial resolution of the product limits its ability to provide spatial patterns of snow cover data. Terra/Aqua with MODIS imager offers a finer resolution than AVHRR at 500 m, though still too coarse for snow-dominated ecosystems, and it has only been available since the 2000s. Landsat offers a balance with high spatial resolution and 40 years of measurements, though their weekly or monthly measurement intervals pose limitations for snow cover monitoring, especially given that cloud cover probability can exceed 50% in temperate mountains[36,37]. AVHRR sensors have been used to investigate snow cover duration trends since 1985 in the European Alps[28]. MODIS has shown a negative trend in snow cover duration of 17 days per decade since 2000 in the Alpine region[38]. Sentinel-2 satellites can produce snow cover maps at 20 m resolution, but their short time span prevents trend analysis[39,40]. To monitor snow cover changes at appropriate spatial and temporal scale, long-term (multi-decadal) time series of consistent and medium resolution (multi-decametric) data are needed[32]. Landsat meets these criteria, but the limited number of observations before the 2000s poses challenges for applications in mountain ecosystems[41]. Figure 1a shows snow melt-out date estimates from MODIS, Sentinel-2 and Landsat for the year 2018 near the Col du Lautaret, France, highlighting the diversity of products available along with their respective advantages and limitations.

In this paper, we present a method and dataset that address the low observation density of Landsat time series by aggregating several years into two 12-year periods: one corresponding to the beginning of the Landsat series (1985–1996), the other to the end (2011–2022) (Fig. 1b). This approach allows densification of the time series and provides a reliable estimate of the SMOD at 30 m resolution. By comparing the SMOD estimates from both periods, our product characterizes changes in SMOD over the last four decades at 30 m spatial resolution and across the main ranges of the European temperate mountain ranges (Pyrenees, European Alps, and Greater Caucasus) (Fig. 2). This method has allowed assessment of the consequences of decreasing snow cover coupled with rising air temperatures on above-treeline vegetation in a separate study[42]. Our findings show that the reduction in snow cover duration has a greater influence on accumulated heat during the growing season than the effect of increased air temperatures only, identifying this heat accumulation as the primary driver of observed greening in late snow-melting sites[42]. Here, we extended the evaluation of the dataset by (1) increasing the number of snow depth stations, and by (2) assessing SMOD uncertainty along mesotopographic and vegetation gradient. This dataset has potential applications beyond alpine ecology research, serving as a valuable resource for studies of snow cover change in poorly instrumented areas of Europe. Studies in snow climatology, natural hazards, or water resources, could benefit from this dataset, providing insights into snow cover duration changes over the last four decades at unprecedented spatial resolution. We also share our code allowing for SMOD data production in Google Earth Engine so that it can be employed in other mountain ranges.

## Methods

**Overview of the Landsat-based SMOD estimates algorithm.** Obtaining a reliable estimate of the Snow Melt-Out Date (SMOD) using Landsat poses a complex challenge due to its dependency on sampling frequency. The combination of a long revisiting time and frequent cloud cover typically results in 1 to 3 observations per month over the European temperate mountains[41]. Additionally, the Landsat time series has irregularities in sampling frequency which are related to the progressive increase in the number of satellites in orbit and variations in acquisition density. In the 1980s and 1990s, observations were more limited compared to recent years, making the estimation process even more challenging. To address these difficulties, we developed a novel method for SMOD estimates by aggregating the Landsat time series.

We utilized all available Tier 1 data from 1984 to 2023 in Landsat Collection 2 provided by the U.S. Geological Survey (USGS) and hosted on Google Earth Engine (GEE) over three mountain ranges: the Pyrenees, European

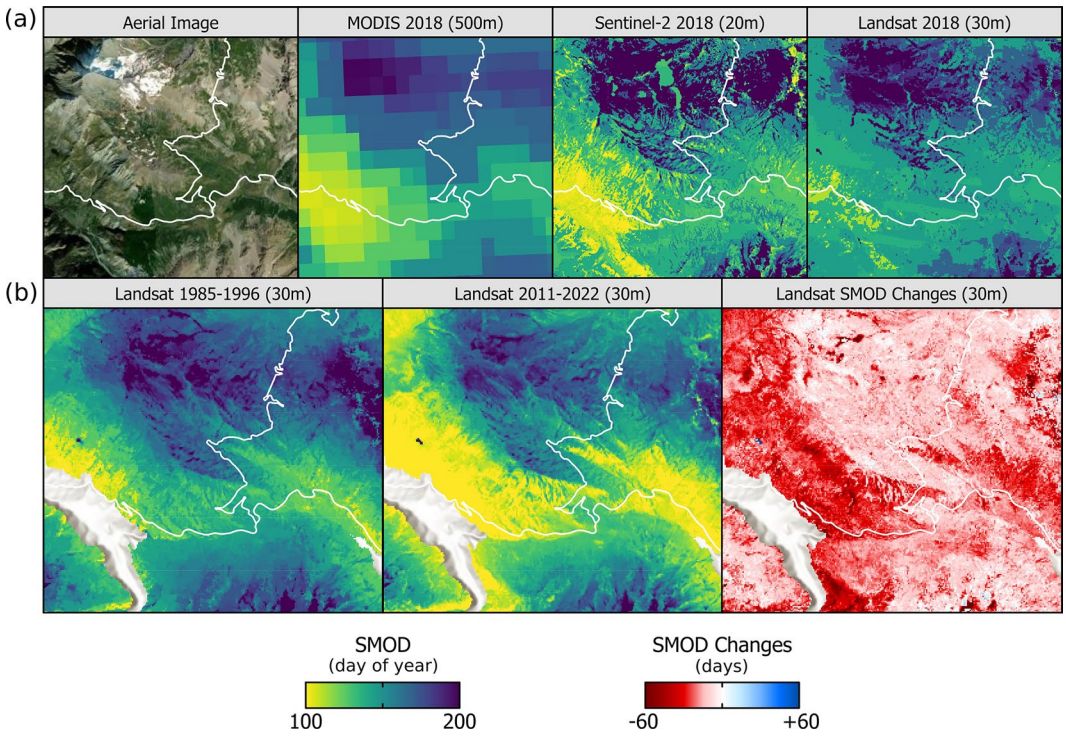


**Fig. 1** Snow melt-out date estimates from satellite remote sensing near the Col du Lautaret, France. (**a**) Snow melt-out dates estimate for the year 2018 using MODIS, Sentinel-2 and Landsat NDSI time series, respectively. MODIS-based SMOD for 2018 was obtained using the MOD10A1.006 collection and computed on GEE. Sentinel-2-based SMOD for 2018 was obtained from Barrou Dumont *et al.*[55]. Landsat-based SMOD for 2018 was derived using the GEE script described in this paper focusing solely on data from the year 2018. (**b**) SMOD estimates for the two Landsat periods (1985–1996 and 2011–2022) obtained by aggregating multiple years of acquisitions showcasing the changes in SMOD between these periods. The area corresponds to the Lautaret Pass in the French Alps with main roads highlighted in white lines.

Alps and Greater Caucasus. The Tier 1 data products analyzed include surface reflectance from Landsat 5 Thematic Mapper (TM), Landsat 7 Enhanced Thematic Mapper + (ETM+) and Landsat 8 Operational Land Imager (OLI). We exclusively selected images with an average cloud cover of less than 80%, as scenes with high cloud cover can compromise the accuracy of geometric calibration. The C Version of Function of Mask (CFmask) was applied to categorize each pixel as clear (land/water), snow, cloud, adjacent to cloud, or cloud shadow[43,44]. Pixels affected by snow, cloud, adjacent to cloud or cloud shadow were excluded from analysis.

We generated an annual time series of Normalized Difference Snow Index (NDSI) computed using corrected green and SWIR1 bands from 1985 to 1996 (Period 1, hereafter referred to as P1) and from 2011 to 2022 (Period 2, hereafter referred to as P2). These years were then aggregated based on the day of year (DOY), resulting in a densified NDSI time series for each 12-year period. We binarized NDSI using an optimal threshold of 0.1543, determined from an extensive dataset of clear-sky Landsat images across the three main mountain ranges of the European temperature mountains (detailed below). Moving window smoothing was then applied to the binarized NDSI time series using a 25-day window length, thereby obtaining a "probability of snow" index. We identified the first observation with a probability lower than 0.5 as the SMOD, starting from DOY 50 to avoid detecting earlier DOY due to snow onset later than January 1. Figure 3 shows the impact of aggregating years on the observation density for a given point, and on the resulting differences in the quality of the SMOD estimate at the pixel scale, with and without aggregation.

**Optimal NDSI threshold for SMOD estimates.** We performed an analysis to determine the optimal NDSI threshold within the context of European temperate mountains for Landsat 5 TM, 7 ETM+ and 8 OLI from Collection 2 at Surface reflectance level. In partially snow-covered images, NDSI follows a bimodal distribution: one mode appears at high NDSI values, corresponding to fully snow-covered pixels; the second one appears at low/negative NDSI values, corresponding to fully snow-free pixels. In winter, the distribution typically shows a high frequency mode at high values, as most of the image is snow-covered. As the season progresses, the frequency increases towards lower values, indicating the gradual melting of snow which changes the asymmetry of the distribution over time.

Applying a threshold to discriminate between "snow-free" and "snow-covered" conditions generally involves selecting a value within this range. Due to the bimodal nature of the NDSI distribution in snow cover areas, the "optimal" threshold can be theoretically estimated using threshold approaches such as Otsu's method[45], which has been applied in several studies[46,47]. We conducted this analysis at a much larger scale to determine

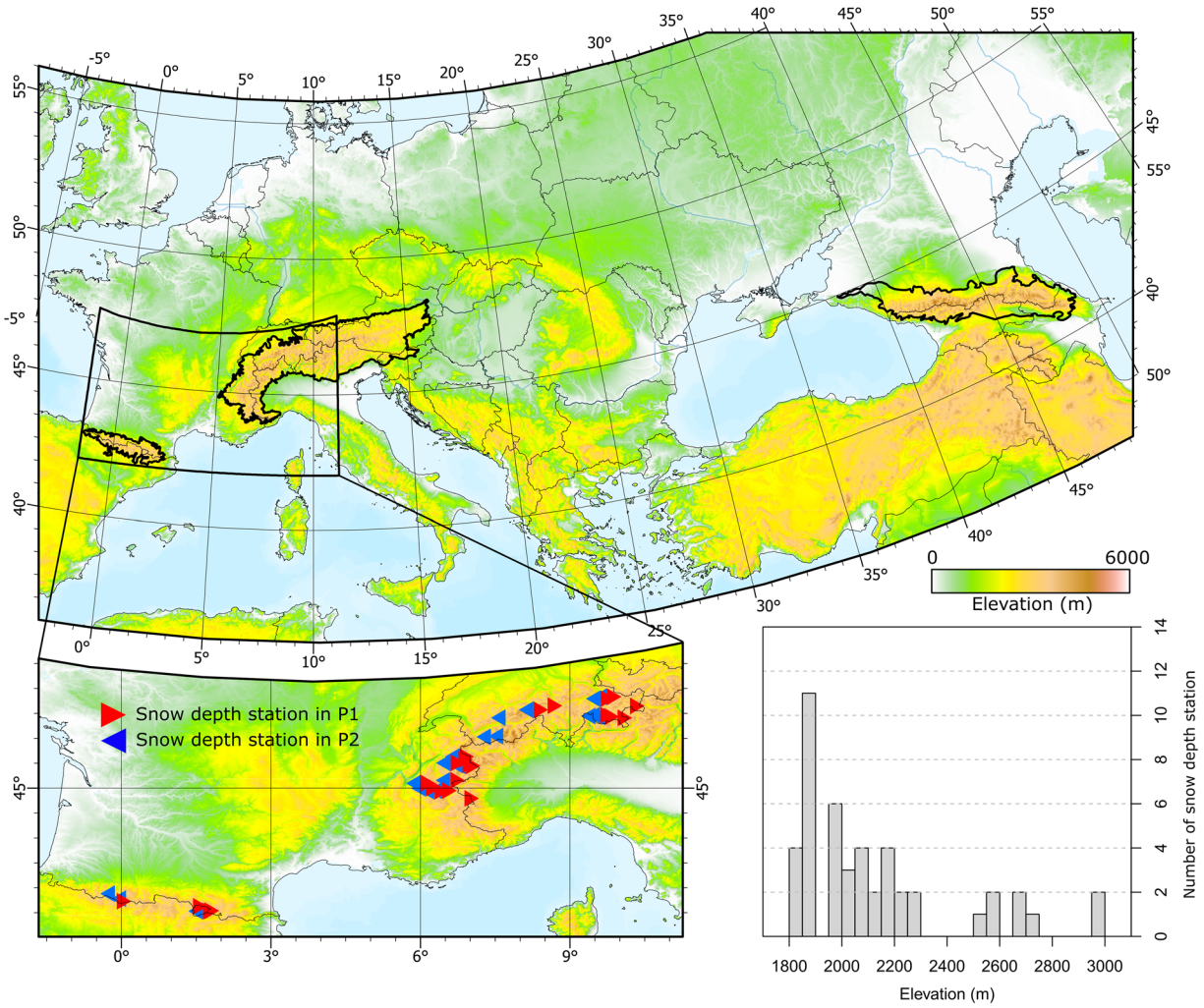


**Fig. 2** Temperate mountains of Europe and high elevation snow depth station used in this study. Location of mountains on which SMOD estimates have been generated at 30 × 30 m spatial resolution using Landsat time series. Red and blue triangles show locations of snow depth stations used to validate our product for both periods. The histogram shows the elevational distribution of the snow depth stations.

the optimal NDSI threshold for the European temperate mountains, and to investigate differences among sensors. For this analysis, we extracted Landsat images from Google Earth Engine using the following criteria: (1) from 1984 to 2023, (2) scene cloud cover < 5%, (3) from April 1 to September 1, (4) over the three mountain ranges included in our study. This yielded a total of 1,866 Landsat images, with 698, 757 and 411 images from Landsat 5 TM, 7 ETM+ and 8 OLI, respectively. To avoid misclassification of snow as clouds, we did not apply a cloud mask; instead, we used a very restrictive threshold for the scene cloud cover. We masked pixels under 1,800 m a.s.l. to minimize the influence of forest cover on our NDSI threshold estimates. Otsu's method requires the existence of a clear bimodal distribution to function effectively. Therefore, we performed a bimodal coefficient test[47] to remove inappropriate images, such as those that were fully cloud-covered or entirely snow-free or snow-covered. In these cases, the NDSI distribution does not display a bimodal pattern, rendering Otsu's method unreliable. We excluded images with a bimodal coefficient <0.85[48] resulting in a final dataset of 121 images, with 39, 49 and 33 images from Landsat 5 TM, 7 ETM+ and 8 OLI, respectively.

First, we used a kernel density estimator to detect the position of the two modes in the NDSI distribution. The NDSI values corresponding to fully snow-free pixels were approximately -0.49 [−0.51/−0.47] (corresponding to median and inter-quartile range), while those for fully snow-covered pixels were around 0.91 [0.89/0.95] which aligns with values reported in the literature[46,49] (Fig. 4a). We found no significant differences in NDSI values for snow-covered and snow-free pixels between Landsat sensors, with values of 0.91 [0.89/0.93], 0.91 [0.89/0.95], and 0.93 [0.91/0.95 for snow-covered pixels and −0.47 [−0.51/−0.45], −0.49 [−0.51/−0.47], and −0.51 [−0.53/−0.47] for snow-free pixels, for Landsat 5, 7 and 8 respectively (Fig. 4b). Next, we systematically computed the optimal NDSI threshold to separate the two modes using Otsu's method utilizing the auto_thresh function from the autothresholdr R package[50]. The average optimal NDSI threshold considering all three sensors was found to be 0.1543 (Fig. 4c) The optimal threshold slightly varied among sensors, with values of 0.1403,

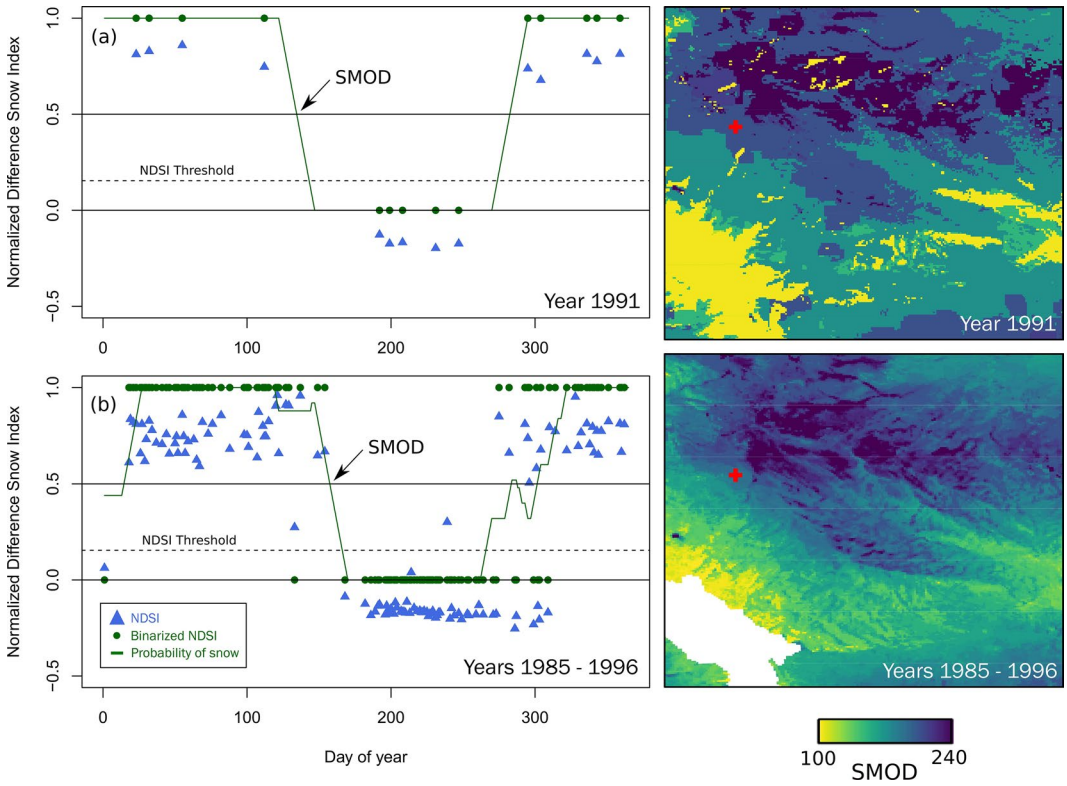


**Fig. 3** Method for estimating Landsat-based SMOD from NDSI time series. Time series of the Normalized Difference Snow Index (NDSI) are presented for the year 1991 (**a**) and for the period 1985–1996 (**b**) within the high-elevation watershed of Roche Noire near Lautaret Pass (France). The pixel location corresponding to the time series displayed on the left is marked with a red cross. This comparison highlights that aggregating multiple years allows capturing SMOD variability at fine spatial scales. The probability of snow corresponds to 25-days running window of binarized NDSI. This illustration is a modified version of supplemental figure 12 in Choler *et al*. (2025).

0.1609 and 0.1496 for Landsat 5, 7 and 8 respectively. Given the minimal differences among sensors, we chose to binarize NDSI using a single threshold of 0.1543.

## Data Records

This dataset[51] has been uploaded to Zenodo and is publicly accessible via https://doi.org/10.5281/zenodo.13151801. It provides information on SMOD at two periods spanning four decades (1985–1996 and 2011–2022), at 30 m spatial resolution for the three main European mountain ranges, the Pyrenees, the European Alps and the Great Caucasus. The data is provided in the ETRS89-extended / LAEA Europe coordinate reference system (EPSG:3035).

The dataset consists of 15 separate GeoTIFF files, categorized as follows: two SMOD files per period and mountain range (one with masks described in the Domain of validity section, one without), and one SMOD change file per mountain range. Filenames are encoded with the first and last year of the period covered, and the mountain range abbreviation (EUALPS, PYRENE and GRTCAU for the European Alps, the Pyrenees and the Greater Caucasus). Files with applied mask ends with "*_MASKED.tif",while those without mask ends with "*_RAW.tif". The files ending in RAW are direct outputs of the GEE script. Users are strongly encouraged to read the technical validation and usage notes provided with the dataset to fully understand the strengths and limitations of the product.

## Technical Validation

**Domain of validity (Pixel selection).** Our data set encompasses the Pyrenees, European Alps and Greater Caucasus Mountain ranges, excluding pixels at elevations below 1800 m asl. Within this area, we have characterized the domain of validity of our product using five criteria: (1) absence of forest cover, (2) no permanent water, ice or snow, (3) observations between May 1 and August 31, (4) absence of penumbra due to cast shadows, and (5) sufficient Landsat observations over the period. These conditions were established as part of an analysis of late snow-melting sites. Noteworthy, pixels outside these conditions may be suitable for analysis. For example, SMOD estimates may be still valid before May 1, below 1800 m and under deciduous forests. The data are also provided without masks, allowing users to define their own range of validity.

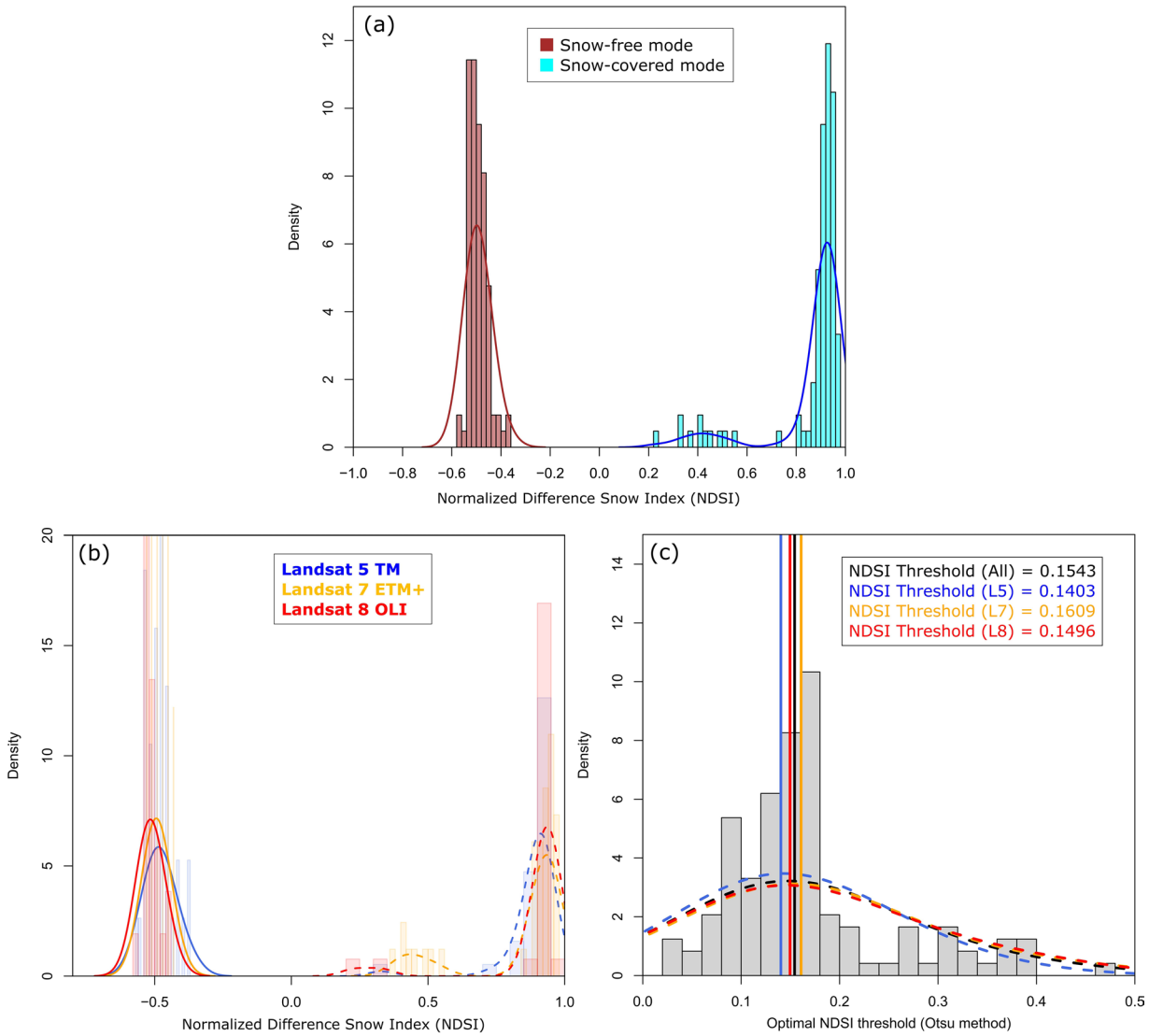


**Fig. 4** Distribution of NDSI values in partially snow-covered areas and optimal NDSI threshold for snow discrimination. (**a**) Distribution of NDSI values for pure snow-free and snow-covered pixels considering all Landsat sensors. (**b**) Distribution of NDSI values of pure snow-free and snow-covered pixels for each Landsat sensor. **(c)** Distribution of optimal NDSI threshold for all sensors (black lines and gray histogram), for Landsat 5 TM (blue), for Landsat 7 ETM+ (orange) and Landsat 8 OLI (red). Dashed lines represent density lines while vertical lines indicate median optimal NDSI thresholds. This figure is a modified version of supplementary figures 10 and 11 in Choler *et al.* (2025).

**Handling of forest and permanent snow/ice cover.** SMOD estimates from satellite remote sensing are generally of poor quality over forested areas. Since the forest cover extends above our elevation threshold, we utilized the JRC Global Forest Cover 2020 V1 product to exclude all pixels covered by forest[52]. Using our SMOD detection method, pixels that consistently show snow cover during the summer were assigned aDOY of 365 interpreted as permanent snow and ice bodies and excluded from the dataset. Water bodies, which also fall into this category (DOY = 365) were removed as well. Given that our SMOD detection algorithm starts at DOY = 50, SMOD estimates close to this date are necessarily less accurate since the function requires a sufficient number of snowy days to accurately detect the absence of snow. Consequently, we retained only pixels between DOY = 121 (May 1), and DOY = 243 (August 31) focusing the product on above-forest ecosystems.

**Impact of cast shadows.** In mountainous regions, reflectance values can be significantly affected by cast shadows leading to distorted SMOD estimates. Although several algorithms can correct for radiometric alterations due to self-shadow[53], cast shadows typically cause complete umbra, resulting in highly disturbed radiometric signals. Identifying these pixels using geometric algorithms that consider solar azimuth and zenith angles is essential, particularly given changes in Landsat image acquisition times over the past 40 years. The trend towards capturing images later in the morning in more recent periods has altered solar zenith and azimuth angles, changing the extent and direction of shadows.

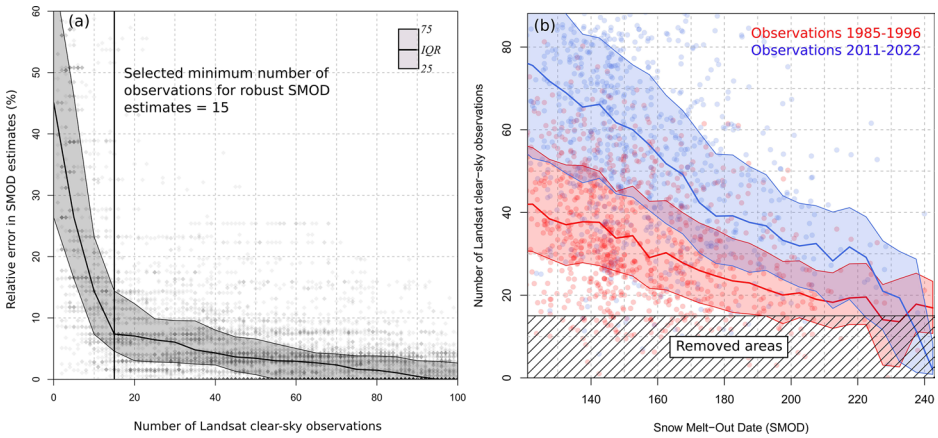


**Fig. 5** Sensitivity of SMOD estimates to the number of clear-sky observations. (**a**) We iteratively computed the Snow Melt-Out Date (SMOD) for a specified extent by systematically excluding one year at a time, thus reducing the number of observations used for SMOD estimation. The SMOD estimates from each iteration were then compared to the "true" SMOD estimates, defined as those estimated using all available observations, across 10,000 pixels. Relative differences between the iteratively calculated SMOD estimates and the "true" SMOD estimates were subsequently computed. (**b**) The number of Landsat clear-sky observations available between March 1 and August 31 is shown for the two study periods. The decline in observation availability as SMOD increases is attributed to rising cloud cover with elevation. This phenomenon is distinct from season length, as snow cover was not excluded from analysis. This figure is a modified version of supplementary figures 9 and 13 in Choler *et al.* (2025).

To address this, we excluded pixels which are often shaded. We computed cast shadows for each Landsat scene from day 121 to 242 of 1996 using the SRTM V3 Digital Elevation Model (30 m resolution), and solar azimuth and zenith angles obtained from Landsat metadata. The year 1996 was selected for this analysis due to its earliest acquisition time (9:20 am), which resulted in the largest extent of cast shadows. For each Landsat scene, we generated a binary raster with value 1 indicating pixels free from cast shadows between DOY 121 and 243. Pixels free from shadows in less than 10% of the scenes (mean value above 0.9) were retained, this threshold was chosen based on visual observations of radiometric distortions. We repeated this analysis for the year 2021 to account for changes in cast shadow direction due to shifts in solar azimuth angles. We applied 1996 and 2021 masks to both periods.

We performed a sensitivity analysis of SMOD to assess the impact of the number of available clear-sky observations on SMOD estimates over the 12-year period. This analysis involved iteratively computing SMOD for a specific duration by systematically excluding one year at a time. As a result, the number of observations utilized for estimating SMOD was progressively reduced. The SMOD estimates from each iteration were then compared to the "true" SMOD estimates (defined as SMOD estimated using all observations) for 10,000 pixels, and relative differences were computed. This method allowed us to quantify the relative error of SMOD estimates across a range of numbers of observations. Our findings revealed that below 15 observations, SMOD estimates linearly deteriorate with the number of observations. Above 15 observations, SMOD estimates exhibit a maximum relative error of +/- 7.5% (Fig. 5a). Consequently, we excluded pixels with less than 15 observations (Fig. 5b).

**Validation of SMOD estimates using snow depth station.** We validated the Landsat-based SMOD estimates from the first and second periods by comparing them with SMOD derived from snow depth station datasets in the Pyrenees and the European Alps. Snow depth station datasets from France were obtained from Météo-France and gap-filled using climate models in order to reconstruct continuous snow depth time series. Snow depth stations from Switzerland were sourced from the MeteoSwiss IDAWEB portal. We included snow depth stations located above 1800 m and having data covering at least one of the two periods. To ensure data quality, we visually inspected each snow depth time series and excluded stations with excessive data gaps. Given that many time series contained significant gaps over the 12-year periods, we ultimately selected 23 snow depth time series covering the first (1985–1996) and 23 covering the second period (2011–2022) (Fig. 2). For each series, we determined the SMOD on annual basis by identifying the first day of the year when snow depth dropped below 5 cm, a threshold chosen to closely match the NDSI value previously determined according to Poussin *et al.* (2023). The median of annual SMOD was computed for each series and compared to Landsat-based SMOD. We found strong agreement between the Landsat-based SMOD estimates and snow depth-derived SMOD, with $R^2$ values of 0.7315 and 0.8594, and a Mean Absolute Error (MAE) of 8 and 6 days, for the first and second period respectively (Fig. 6). These results underscore the robustness of our SMOD estimates, particularly for the first period, which had a limited number of clear-sky observations. In addition, the consistent performance of SMOD estimates across both periods further supports their use in assessing SMOD changes over time.

**Validation of SMOD estimates using soil temperature loggers.** We further validated the Landsat-based SMOD estimates for the second period (2011–2022) using SMOD data derived from soil temperature loggers which recorded almost continuous data from 2011 to 2022[54]. All loggers were located in the eLTER

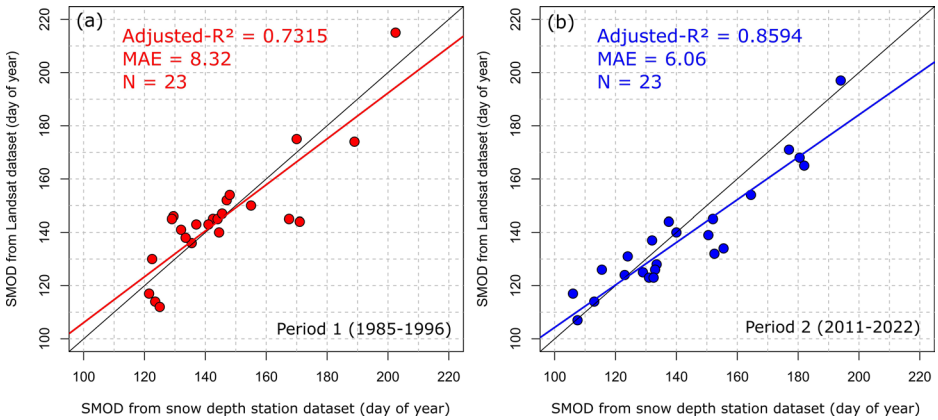


**Fig. 6** Evaluation of Landsat-based SMOD using snow depth station dataset. Comparison was made using snow depth station dataset from Pyrenees and European Alps. SMOD was estimated as the first day when a snow depth dropped below 5 cm, for (**a**) the first period (1985–1996) and (**b**) the second period (2011–2022). MAE: Mean Absolute Error.

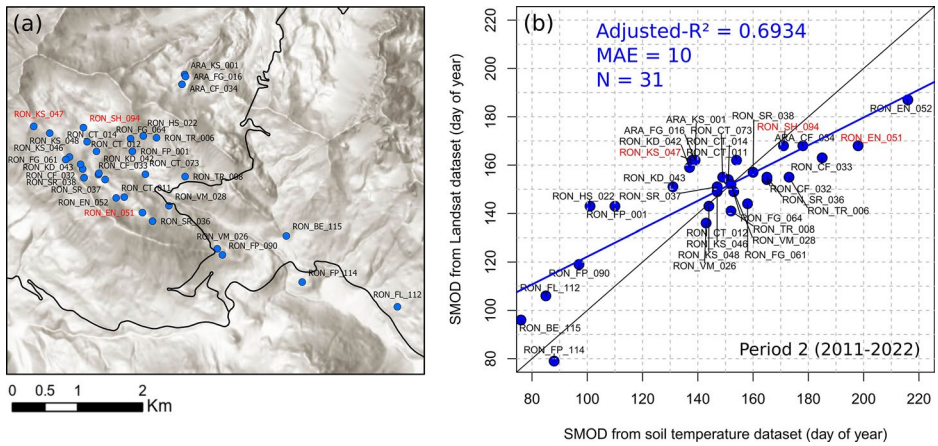


**Fig. 7** Evaluation of Landsat-based SMOD using soil temperature loggers. (**a**) Distribution of the 31 loggers with 12 years of data (2011–2022) near Col du Lautaret. (**b**) Comparison between SMOD derived from soil temperature loggers (defined as the first day when soil temperature exceeds 1 °C) and SMOD from Landsat dataset for the second period (2011–2022). Site names highlighted in red correspond to those displayed in Fig. 8. Soil temperature site names can be linked to site information by referring to Choler[54].

site Lautaret-Rochenoire in the French Alps (Fig. 7a). This dataset allowed evaluation of our 30-m spatial resolution SMOD along mesotopographic gradients and different vegetation contexts.

We found a good agreement between the Landsat-based SMOD estimates and the soil temperature-based SMOD estimates with an $R^2$ of 0.69 and a MAE of 10 days (Fig. 7b). Examination of specific sites with known topographic contexts revealed that the Landsat-based estimates tend to predict SMOD slightly earlier in areas where snow accumulates. This discrepancy is attributed to the positioning of the logger within the Landsat pixel. In such scenarios, the loggers are consistently placed in locations where snow persists the longest, while Landsat provides an estimation of SMOD at the pixel scale, giving limited weight to the last patch of snow within the pixel (as the NDSI threshold is crossed well before the final melting date). In Fig. 8, We present four examples of soil temperature logger time series and NDSI time series for the pixel overlapping each logger, corresponding to gradients of micro-topography.

## Usage Notes

This dataset provides researchers with information on snow melt-out dates over two periods spanning four decades, at an unprecedented spatial resolution suitable for alpine ecosystems. The product has been designed for alpine ecology and some methodological choices may not be optimal for other applications such as climatology, risk assessment or hydrology). The GEE script used to produce this dataset is freely accessible to the community, and many parameters can be adjusted to suit different research needs. For example, SMOD estimates can be produced over a shorter time window, as long as the number of observations is sufficient for reliable estimates, or over different time periods. Our analysis indicates that a minimum of 15 observations between May 1 and

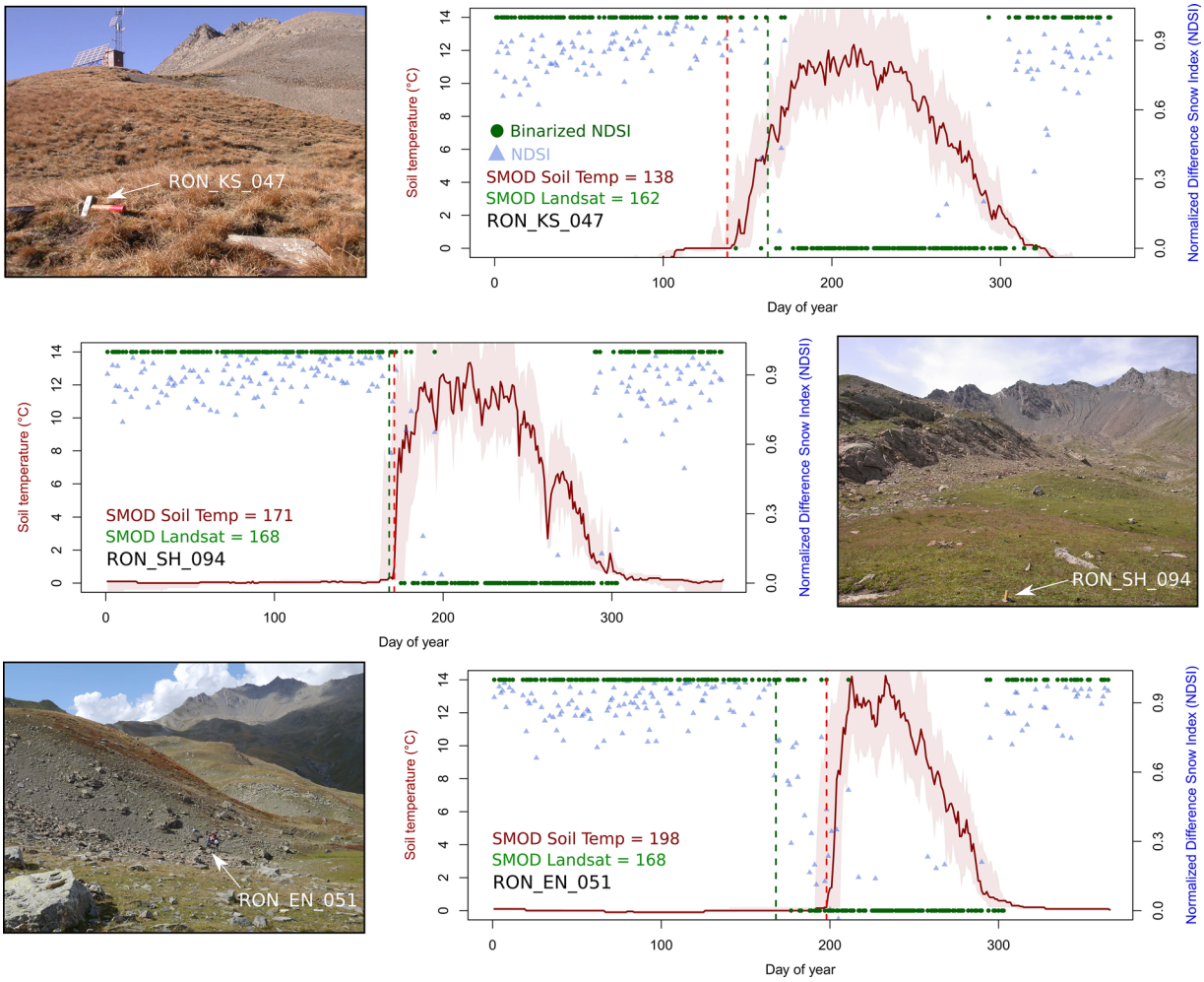


**Fig. 8** Comparison of soil temperature and NDSI time series for three plant communities in contrasting topographic contexts. (**a**) Soil temperature and NDSI time series for site RON_KS_047 representing crest communities dominated by *Carex myosuroides*. (**b**) Soil temperature and NDSI time series for site RON_SH_094 representing plant communities dominated by *Salix herbacea*. (**c**) Soil temperature and NDSI time series for the RON_EN_051 site representing sparsely vegetated late snow-melting site dominated by *Alopecurus gerardi*. Red solid lines correspond to median soil temperature over available years and shadowed area corresponds to inter-quartile ranges.

August 31 is necessary to obtain reliable SMOD estimates. The 12-year window chosen for this study allows us to meet this observation requirement in late snow melting ecosystems, where observations are the most limited. Researchers focusing on subalpine ecosystems could potentially shorten this window and still achieve reliable SMOD estimates. Conversely, regions like Alaska, where Landsat observations are more restricted especially in earlier periods, may require longer observation windows to obtain accurate SMOD estimates.

## Code availability

The algorithm used for obtaining SMOD estimates was developed in Google Earth Engine and is freely available here and can be used to reproduce the SMOD data without masks described in the Domain of validity section.
https://code.earthengine.google.com/9eb2a7223bd3ebb8fc857e79990bfca4?noload=true.

Received: 18 November 2024; Accepted: 22 April 2025;
Published online: 29 April 2025

## References

1. Copernicus, C. S. Global Climate Highlights. (2023).
2. Beniston, M. & Stoffel, M. Assessing the impacts of climatic change on mountain water resources. *Sci Total Environ* **493**, 1129–1137, https://doi.org/10.1016/j.scitotenv.2013.11.122 (2014).
3. Gobiet, A. *et al*. 21st century climate change in the European Alps–a review. *Sci Total Environ* **493**, 1138–1151, https://doi.org/10.1016/j.scitotenv.2013.07.050 (2014).
4. Switanek, M. *et al*. Snow depth sensitivity to mean temperature, precipitation, and elevation in the Austrian and Swiss Alps. *The Cryosphere* **18**, 6005–6026, https://doi.org/10.5194/tc-18-6005-2024 (2024).

5. Inouye, D. W. Effects of climate change on phenology, frost damage, and floral abundance of montane wildflowers. *Ecology* **89**, 353–362, https://doi.org/10.1890/06-2128.1 (2008).
6. Wipf, S. & Rixen, C. A review of snow manipulation experiments in Arctic and alpine tundra ecosystems. *Polar Research* **29**, 95–109, https://doi.org/10.1111/j.1751-8369.2010.00153.x (2010).
7. Choler, P. Winter soil temperature dependence of alpine plant distribution: Implications for anticipating vegetation changes under a warming climate. *Perspectives in Plant Ecology, Evolution and Systematics* **30**, 6–15, https://doi.org/10.1016/j.ppees.2017.11.002 (2018).
8. Sturm, M. *et al*. Winter Biological Processes Could Help Convert Arctic Tundra to Shrubland. *BioScience* **55**, 17, https://doi.org/10.1641/0006-3568(2005)055[0017:wbpchc]2.0.co;2 (2005).
9. Baptist, F., Yoccoz, N. G. & Choler, P. Direct and indirect control by snow cover over decomposition in alpine tundra along a snowmelt gradient. *Plant and Soil* **328**, 397–410, https://doi.org/10.1007/s11104-009-0119-6 (2009).
10. Choler, P., Michalet, R. & Callaway, R. M. Facilitation and Competition on Gradients in Alpine Plant Communities. *Ecology* **82**, 3295–3308, https://doi.org/10.1890/0012-9658(2001)082[3295:facogi]2.0.co;2 (2001).
11. Baptist, F. & Choler, P. A simulation of the importance of length of growing season and canopy functional properties on the seasonal gross primary production of temperate alpine meadows. *Ann Bot* **101**, 549–559, https://doi.org/10.1093/aob/mcm318 (2008).
12. Wundram, D., Pape, R. & Löffler, J. Alpine Soil Temperature Variability at Multiple Scales. *Arctic, Antarctic, and Alpine Research* **42**, 117–128, https://doi.org/10.1657/1938-4246-42.1.117 (2010).
13. Notarnicola, C. Overall negative trends for snow cover extent and duration in global mountain regions over 1982-2020. *Sci Rep* **12**, 13731, https://doi.org/10.1038/s41598-022-16743-w (2022).
14. Notarnicola, C. Hotspots of snow cover changes in global mountain regions over 2000–2018. *Remote Sensing of Environment* **243**, 111781, https://doi.org/10.1016/j.rse.2020.111781 (2020).
15. López-Moreno, J. I. *et al*. Long-term trends (1958–2017) in snow cover duration and depth in the Pyrenees. *International Journal of Climatology* **40**, 6122–6136, https://doi.org/10.1002/joc.6571 (2020).
16. Pons, M. R., San-Martín, D., Herrera, S. & Gutiérrez, J. M. Snow trends in Northern Spain: analysis and simulation with statistical downscaling methods. *International Journal of Climatology* **30**, 1795–1806, https://doi.org/10.1002/joc.2016 (2009).
17. Durand, Y. *et al*. Reanalysis of 47 Years of Climate in the French Alps (1958–2005): Climatology and Trends for Snow Cover. *Journal of Applied Meteorology and Climatology* **48**, 2487–2512, https://doi.org/10.1175/2009jamc1810.1 (2009).
18. Matiu, M. *et al*. Observed snow depth trends in the European Alps: 1971 to 2019. *The Cryosphere* **15**, 1343–1382, https://doi.org/10.5194/tc-15-1343-2021 (2021).
19. Laternser, M. & Schneebeli, M. Long-term snow climate trends of the Swiss Alps (1931–99). *International Journal of Climatology* **23**, 733–750, https://doi.org/10.1002/joc.912 (2003).
20. Marcolini, G., Bellin, A., Disse, M. & Chiogna, G. Variability in snow depth time series in the Adige catchment. *Journal of Hydrology: Regional Studies* **13**, 240–254, https://doi.org/10.1016/j.ejrh.2017.08.007 (2017).
21. Valt, M. & Cianfarra, P. Recent snow cover variability in the Italian Alps. *Cold Regions Science and Technology* **64**, 146–157, https://doi.org/10.1016/j.coldregions.2010.08.008 (2010).
22. Serquet, G., Marty, C., Dulex, J.-P. & Rebetez, M. Seasonal trends and temperature dependence of the snowfall/precipitation-day ratio in Switzerland. *Geophysical Research Letters* **38**, n/a–n/a, https://doi.org/10.1029/2011gl046976 (2011).
23. Urban, G., Richterová, D., Kliegrová, S. & Zusková, I. Reasons for shortening snow cover duration in the Western Sudetes in light of global climate change. *International Journal of Climatology* **43**, 5485–5511, https://doi.org/10.1002/joc.8157 (2023).
24. Klein, G., Vitasse, Y., Rixen, C., Marty, C. & Rebetez, M. Shorter snow cover duration since 1970 in the Swiss Alps due to earlier snowmelt more than to later snow onset. *Climatic Change* **139**, 637–649, https://doi.org/10.1007/s10584-016-1806-y (2016).
25. Robinson, D. A. & Frei, A. Seasonal Variability of Northern Hemisphere Snow Extent Using Visible Satellite Data. *The Professional Geographer* **52**, 307–315, https://doi.org/10.1111/0033-0124.00226 (2010).
26. Reid, P. C. *et al*. Global impacts of the 1980s regime shift. *Glob Chang Biol* **22**, 682–703, https://doi.org/10.1111/gcb.13106 (2016).
27. Scherrer, S. C., Wüthrich, C., Croci-Maspoli, M., Weingartner, R. & Appenzeller, C. Snow variability in the Swiss Alps 1864–2009. *International Journal of Climatology* **33**, 3162–3173, https://doi.org/10.1002/joc.3653 (2013).
28. Hüsler, F., Jonas, T., Riffler, M., Musial, J. P. & Wunderle, S. A satellite-based snow cover climatology (1985–2011) for the European Alps derived from AVHRR data. *The Cryosphere* **8**, 73–90, https://doi.org/10.5194/tc-8-73-2014 (2014).
29. Monteiro, D. & Morin, S. Multi-decadal analysis of past winter temperature, precipitation and snow cover data in the European Alps from reanalyses, climate models and observational datasets. *The Cryosphere* **17**, 3617–3660, https://doi.org/10.5194/tc-17-3617-2023 (2023).
30. Mendoza, P. A. *et al*. Interannual and Seasonal Variability of Snow Depth Scaling Behavior in a Subalpine Catchment. *Water Resources Research* **56**, https://doi.org/10.1029/2020wr027343 (2020).
31. Trujillo, E., Ramírez, J. A. & Elder, K. J. Topographic, meteorologic, and canopy controls on the scaling characteristics of the spatial distribution of snow depth fields. *Water Resources Research* **43**, https://doi.org/10.1029/2006wr005317 (2007).
32. Dedieu, J.-P. *et al*. On the Importance of High-Resolution Time Series of Optical Imagery for Quantifying the Effects of Snow Cover Duration on Alpine Plant Habitat. *Remote Sensing* **8**, 481, https://doi.org/10.3390/rs8060481 (2016).
33. Hantel, M., Maurer, C. & Mayer, D. The snowline climate of the Alps 1961–2010. *Theoretical and Applied Climatology* **110**, 517–537, https://doi.org/10.1007/s00704-012-0688-9 (2012).
34. Masson-Delmotte, V., *et al* (eds.). IPCC, 2021: Climate Change 2021: The Physical Science Basis. Contribution of Working Group I to the Sixth Assessment Report of the Intergovernmental Panel on Climate Change. (2021).
35. Dietz, A. J., Kuenzer, C., Gessner, U. & Dech, S. Remote sensing of snow – a review of available methods. *International Journal of Remote Sensing* **33**, 4094–4134, https://doi.org/10.1080/01431161.2011.640964 (2011).
36. Gascoin, S. *et al*. A snow cover climatology for the Pyrenees from MODIS snow products. *Hydrology and Earth System Sciences* **19**, 2337–2351, https://doi.org/10.5194/hess-19-2337-2015 (2015).
37. Parajka, J. & Blöschl, G. Spatio-temporal combination of MODIS images – potential for snow cover mapping. *Water Resources Research* **44**, https://doi.org/10.1029/2007wr006204 (2008).
38. Fugazza, D., Manara, V., Senese, A., Diolaiuti, G. & Maugeri, M. Snow Cover Variability in the Greater Alpine Region in the MODIS Era (2000–2019). *Remote Sensing* **13**, https://doi.org/10.3390/rs13152945 (2021).
39. Gascoin, S., Grizonnet, M., Bouchet, M., Salgues, G. & Hagolle, O. Theia Snow collection: high-resolution operational snow cover maps from Sentinel-2 and Landsat-8 data. *Earth System Science Data* **11**, 493–514, https://doi.org/10.5194/essd-11-493-2019 (2019).
40. Barrou Dumont, Z. *et al*. Brief communication: Evaluation of the snow cover detection in the Copernicus High Resolution Snow & Ice Monitoring Service. *The Cryosphere* **15**, 4975–4980, https://doi.org/10.5194/tc-15-4975-2021 (2021).
41. Bayle, A., Gascoin, S., Berner, L. T. & Choler, P. Landsat-based greening trends in alpine ecosystems are inflated by multidecadal increases in summer observations. *Ecography*, https://doi.org/10.21203/rs.3.rs-4153160/v2 (2024).
42. Choler, P., Bayle, A., Fort, N. & Gascoin, S. Waning snowfields have transformed into hotspots of greening within the alpine zone. *Nature Climate Change* **15**, 80-85, https://doi.org/10.1038/s41558-024-02177-x (2025).
43. Zhu, Z. & Woodcock, C. E. Object-based cloud and cloud shadow detection in Landsat imagery. *Remote Sensing of Environment* **118**, 83–94, https://doi.org/10.1016/j.rse.2011.10.028 (2012).

44. Zhu, Z. & Woodcock, C. E. Automated cloud, cloud shadow, and snow detection in multitemporal Landsat data: An algorithm designed specifically for monitoring land cover change. *Remote Sensing of Environment* **152**, 217–234, https://doi.org/10.1016/j.rse.2014.06.012 (2014).
45. Otsu, N. A Threshold Selection Method from Gray-Level Histograms. *IEEE Transactions on Systems, Man, and Cybernetics* **9**, 62–66, https://doi.org/10.1109/tsmc.1979.4310076 (1979).
46. Yin, D., Cao, X., Chen, X., Shao, Y. & Chen, J. Comparison of automatic thresholding methods for snow-cover mapping using Landsat TM imagery. *International Journal of Remote Sensing* **34**, 6529–6538, https://doi.org/10.1080/01431161.2013.803631 (2013).
47. Härer, S., Bernhardt, M., Siebers, M. & Schulz, K. On the need for a time- and location-dependent estimation of the NDSI threshold value for reducing existing uncertainties in snow cover maps at different scales. *The Cryosphere* **12**, 1629–1642, https://doi.org/10.5194/tc-12-1629-2018 (2018).
48. Pfister, R., Schwarz, K. A., Janczyk, M., Dale, R. & Freeman, J. B. Good things peak in pairs: a note on the bimodality coefficient. *Front Psychol* **4**, 700, https://doi.org/10.3389/fpsyg.2013.00700 (2013).
49. Poussin, C., Timoner, P., Chatenoux, B., Giuliani, G. & Peduzzi, P. Improved Landsat-based snow cover mapping accuracy using a spatiotemporal NDSI and generalized linear mixed model. *Science of Remote Sensing* **7**, 100078, https://doi.org/10.1016/j.srs.2023.100078 (2023).
50. Landini, G., Randell, D. A., Fouad, S. & Galton, A. Automatic thresholding from the gradients of region boundaries. *J Microsc* **265**, 185–195, https://doi.org/10.1111/jmi.12474 (2017).
51. Bayle, A., Gascoin, S., Corona, C., Stoffel, M. & Choler, P. Gridded snow melt-out date (SMOD) dataset for Pyrenees, European Alps and Greater Caucasus at 30-m spatial resolution and two periods, 1985-1996 and 2011-2022. *Zenodo* https://doi.org/10.5281/zenodo.13151801 (2025).
52. Commission, E. *et al*. *Mapping global forest cover of the year 2020 to support the EU regulation on deforestation-free supply chains*. (Publications Office of the European Union, 2024).
53. Sola, I., González-Audícana, M. & Álvarez-Mozos, J. Multi-criteria evaluation of topographic correction methods. *Remote Sensing of Environment* **184**, 247–262, https://doi.org/10.1016/j.rse.2016.07.002 (2016).
54. Choler, P. Long-term monitoring of near-surface soil temperature in mountain ecosystems of the LTSER Lautaret-Oisans. *Recherche Data Gouv*, https://doi.org/10.57745/QCVYG3 (2023).
55. Barrou Dumont, Z. *et al*. Trends in the annual snow melt-out day over the French Alps and the Pyrenees from 38 years of high resolution satellite data (1986–2023). *The Cryosphere*, https://doi.org/10.5194/egusphere-2024-3505 (2025).


## Acknowledgements

A.B. acknowledges a CNRS doctoral scholarship. This work received funding from the European Union's LIFE Programme (project PASTORALP, LIFE16 CCA/IT/000060) and from the Agence Nationale de la Recherche (project TOP, grant no. ANR-20-CE32-0002). Part of this research was supported by the Jardin Alpin du Lautaret, a member of the eLTER Research Infrastructure. LECA acknowledges the Agence Nationale de la Recherche (grant nos. Labex OSUG@2020 and IA-10- LABX-0056).

## Author contributions

A.B. and S.G. worked on the method, processing of remote sensing data and developed the GEE script. P.C. designed the initial study from which emanates this dataset and prepared soil temperature data. C.C. and M.S. prepared the snow depth station dataset from Switzerland. A.B. led the writing. All authors have participated in the writing of the manuscript and have discussed the analyses performed.

## Competing interests

The authors declare no competing interests.

## Additional information

**Correspondence** and requests for materials should be addressed to A.B.

**Reprints and permissions information** is available at www.nature.com/reprints.

**Publisher's note** Springer Nature remains neutral with regard to jurisdictional claims in published maps and institutional affiliations.